Chapter 17B. Analysis of Imaging Spectrometer Data for the Baghlan Area of Interest

By Todd M. Hoefen, Stuart A. Giles, and Raymond F. Kokaly

Abstract

Hyperspectral remote sensing data collected over the Baghlan area of interest (AOI) in northeast central Afghanistan were analyzed with spectroscopic methods to identify the occurrence of selected surficial material classes. Absorption features in the spectra of HyMap data were compared to a reference library of spectra of known materials. Carbonates and vegetation cover most of the Baghlan AOI. Distinct patterns of muscovite, kaolinite, chlorite or epidote, montmorillonite, serpentine, and dolomite + montmorillonite/calcite occur in localized patterns throughout the AOI. HyMap data were found to be an effective tool for detecting and mapping gypsum in areas adjacent to the bedded gypsum prospects at Nalak and Nadr and to a lesser extent at the Kamard and Dasht-i-Safed prospects. Gypsum was also mapped in several other areas throughout the AOI.

17B.1 Introduction

Past studies of geologic data of Afghanistan revealed numerous areas with indications of potential mineral resources of various types (Peters and others, 2007; Abdullah and others, 1977). Several of these areas were selected for follow-on studies using imaging spectroscopy to characterize surface materials. Imaging spectroscopy is an advanced type of remote sensing that is also known as hyperspectral remote sensing. One area selected for study is the Baghlan area of interest (AOI) in northeast central Afghanistan, which is approximately 150 km northwest of Kabul (fig. 17B–1). The area has the potential for clay, gypsum, copper, and bauxite deposits (Peters and others, 2007). To help assess these potential resources, high-resolution imaging spectrometer data were analyzed to detect the presence of selected minerals that may be indicative of past mineralization processes. This report contains the results of the spectroscopic data analyses and identifies sites within the Baghlan AOI that warrant further investigation, especially detailed geological mapping, lithologic sampling, and geochemical studies.

17B.2 Data Collection and Processing

In 2007, imaging spectrometer data were acquired over most of Afghanistan as part of the U.S. Geological Survey (USGS) project “Oil and Gas Resources Assessment of the Katawaz and Helmand Basins.” These data were collected to characterize surface materials in support of assessments of resources (coal, water, minerals, and oil and gas) and earthquake hazards in the country (King and others, 2010). Imaging spectrometers measure the reflectance of visible and near-infrared light from the Earth’s surface in many narrow channels, producing a reflectance spectrum for each image pixel. These reflectance spectra can be interpreted to identify absorption features that arise from specific chemical transitions and molecular bonds that provide compositional information about surface materials. Imaging spectrometer data can only be used to characterize the upper surface materials and not subsurface composition or structure. However, subsurface processes can be indicated by the distribution of surface materials.

17B.2.1 Collection of Imaging Spectrometer Data

The HyMap imaging spectrometer (Cocks and others, 1998) was flown over Afghanistan from August 22 to October 2, 2007 (Kokaly and others, 2008). HyMap has 512 cross-track pixels and covers the wavelength range 0.43 to 2.48 microns (μm) in 128 channels. The imaging spectrometer was flown on a WB-57 high-altitude aircraft at 50,000 ft. There were 207 standard data flight lines and 11 cross-cutting calibration lines collected over Afghanistan for a total of 218 flight lines, covering a surface area of 438,012 km^2 (Kokaly and others, 2008). Data were received in scaled radiance (calibrated to National Institute of Standards and Technology reference materials). Before processing, four channels that had low signal-to-noise and (or) were in wavelength regions that overlapped between detectors were removed from the HyMap data. Each flight line was georeferenced to Landsat Thematic Mapper (TM) base imagery in UTM projection (Davis, 2007).

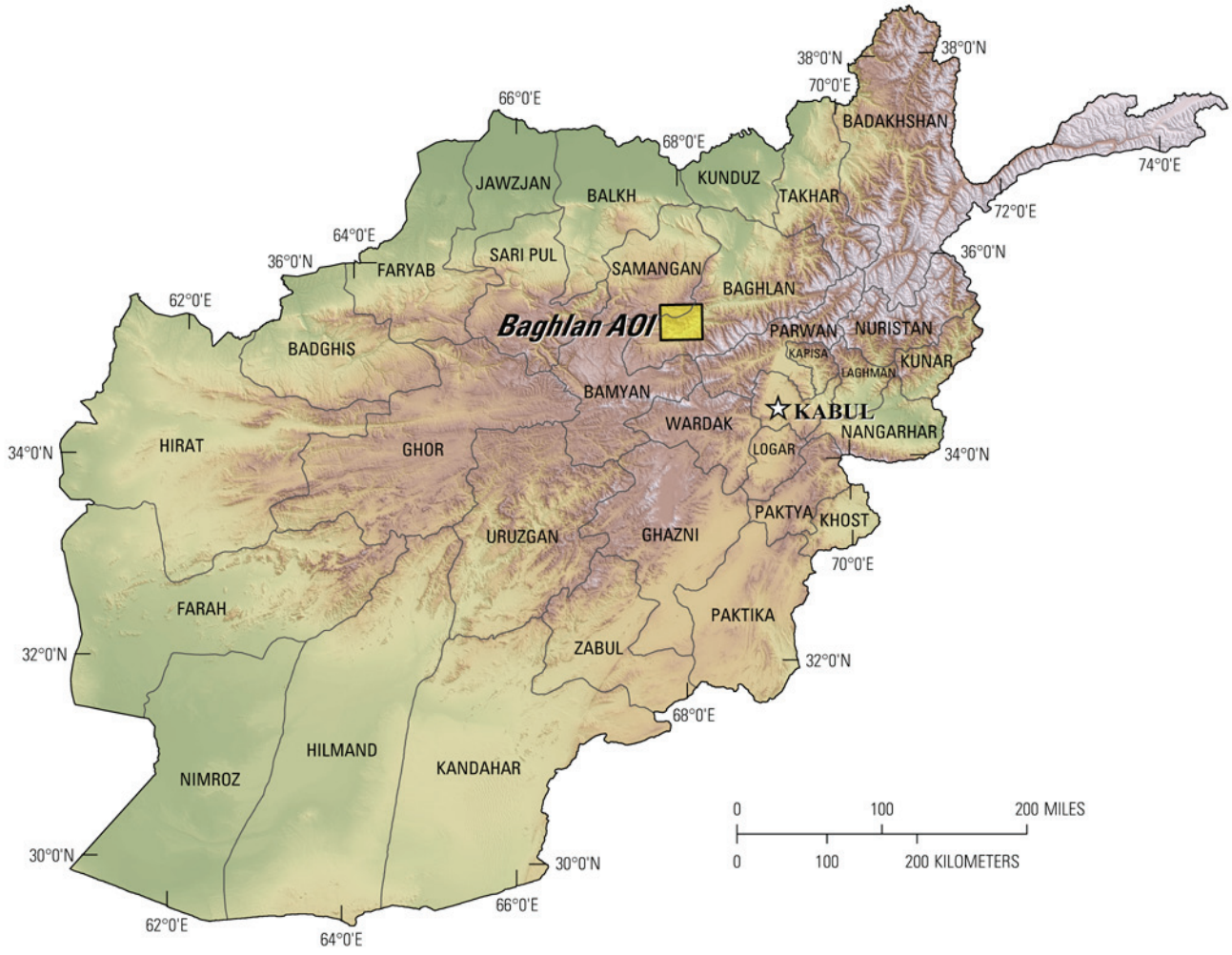

Figure 17B–1. Index map of the Baghlan area of interest (AOI), northeast Afghanistan.

17B.2.2 Calibration

HyMap data were converted from radiance to reflectance using a multi-step process. This calibration process removed the influence of the solar irradiance function, atmospheric absorptions, and residual instrument artifacts, resulting in reflectance spectra that have spectral features that arise from the material composition of the surface. Because of the extreme topographic relief and restricted access to ground-calibration sites, modifications to the typical USGS calibration procedures were required to calibrate the 2007 Afghanistan HyMap dataset (Hoefen and others, 2010). In the first step of the

calibration process, the radiance data were converted to apparent surface reflectance using the radiative transfer correction program Atmospheric CORrection Now (ACORN; ImSpec LLC, Palmdale, Calif.). ACORN was run multiple times for each flight line, using average elevations in 100-m increments, covering the range of minimum to maximum elevation within the flight line. A single atmospherically corrected image was assembled from these elevation-incremented ACORN results. This was done by determining the elevation of each HyMap pixel and selecting the atmospherically corrected pixel from the 100-m increment closest to that elevation.

Each assembled atmospherically corrected image was further empirically adjusted using ground-based reflectance measurements from a ground-calibration site. Spectra of five ground-calibration sites were collected in Afghanistan: Kandahar Air Field, Bagram Air Base, and Mazar-e-Sharif Airport, as well as soil samples from two fallow fields in Kabul. These were used to calculate empirical correction factors using the pixels of atmospherically corrected HyMap data in the flight lines that passed over the sites. The empirical correction from the closest calibration site to each flight line was applied.

To further improve the data quality, an additional calibration step was taken to address the atmospheric differences caused, in part, by the large distances from calibration sites to where the HyMap data were acquired. The large distances were a result of the lack of safe access to ground-calibration sites. The duration of the airborne survey and variation in time of day during which flight lines were acquired also resulted in differences in atmospheric conditions between standard flight lines and lines over ground-calibration sites, which were used to derive the empirical correction factors. During the course of the data collection, the sun angle, atmospheric water vapor, and atmospheric scattering differed for each flight line. To compensate for this, cross-cutting calibration flight lines over the ground-calibration areas were acquired (Kokaly and others, 2008) and used to refine data quality of standard data lines. A multiplier correction for each standard data line, typically oriented north-south, was derived using the pixels of overlap with the well-calibrated cross-cutting line that intersected it, subject to slope, vegetation cover, and other restrictions on pixel selection (Hoefen and others, 2010). As a result, the localized cross-calibration multiplier, derived from the overlap region, corrected residual atmospheric contamination in the imaging spectrometer data that may have been present after the ground-calibration step.

17B.2.3 Materials Maps and Presentation

After undergoing a complex and rigorous data calibration process, the georeferenced and calibrated reflectance data were analyzed using the Material Identification and Characterization Algorithm (MICA), a module of the USGS Processing Routines in IDL (Interactive Data Language) for Spectroscopic Measurements (PRISM) software (Kokaly, 2011). The MICA analysis compared the reflectance spectrum of each pixel of HyMap data to entries in a reference spectral library of minerals, vegetation, water, and other materials. The HyMap data were compared to 97 reference spectra of well-characterized mineral and material standards. The best spectral match to each pixel was determined, and the results were clustered into classes of materials discussed below. The resulting maps of material distribution, resampled to a 23 x 23 meter square pixel grid, were mosaicked to create thematic maps of surface mineral occurrences over the full dataset covering Afghanistan.

MICA was applied to HyMap data twice in order to present the distribution of two categories of minerals that are naturally separated in the wavelength regions of their primary absorption features. MICA was applied using the subset of minerals with absorption features in the visible and near-infrared wavelength region, producing a 1-µm map of iron-bearing minerals and other materials (King, Kukaly, and others, 2011), and again using the subset of minerals with absorption features in the shortwave infrared, producing a 2-µm map of carbonates, phyllosilicates, sulfates, altered minerals, and other materials (Kokaly and others, 2011). For clarity of presentation, some individual classes in these two maps were bundled by combining selected mineral types (for example, all montmorillonites or all kaolinites) and representing them with the same color in order to reduce the number of colors required to represent the mineral classes.

The iron-bearing minerals map has 28 classes. Iron-bearing minerals with different mineral compositions but similar broad spectral features are difficult to classify as specific mineral species. Thus, generic spectral classes, including several minerals with similar absorption features, such as Fe^{3+}, Type 1 and Fe^{3+}, Type 2, are depicted on the map. The carbonate, phyllosilicate, sulfates, and altered minerals map has 32 classes. Minerals with slightly different mineral compositions but comparable spectral features are less easily discriminated; thus, some identified classes consist of several minerals with similar spectra, such as the chlorite or epidote class. When comparisons with reference spectra resulted in no viable match, a designation of "not classified" was assigned to a pixel.

17B.3 Geologic Setting of the Baghlan Area Of Interest

The Baghlan AOI is within the Baghlan and Samangan Provinces in central-northeast Afghanistan. The main Baghlan AOI is approximately 1,800 km^2. The contrast-enhanced stretch of the natural-color composite of Landsat Thematic Mapper bands in figure 17B–2 provides a general overview of the Baghlan AOI terrain and is useful for understanding the general characteristics and distribution of surficial material including rocks and soil, unconsolidated sediments, vegetation, and hydrologic features.

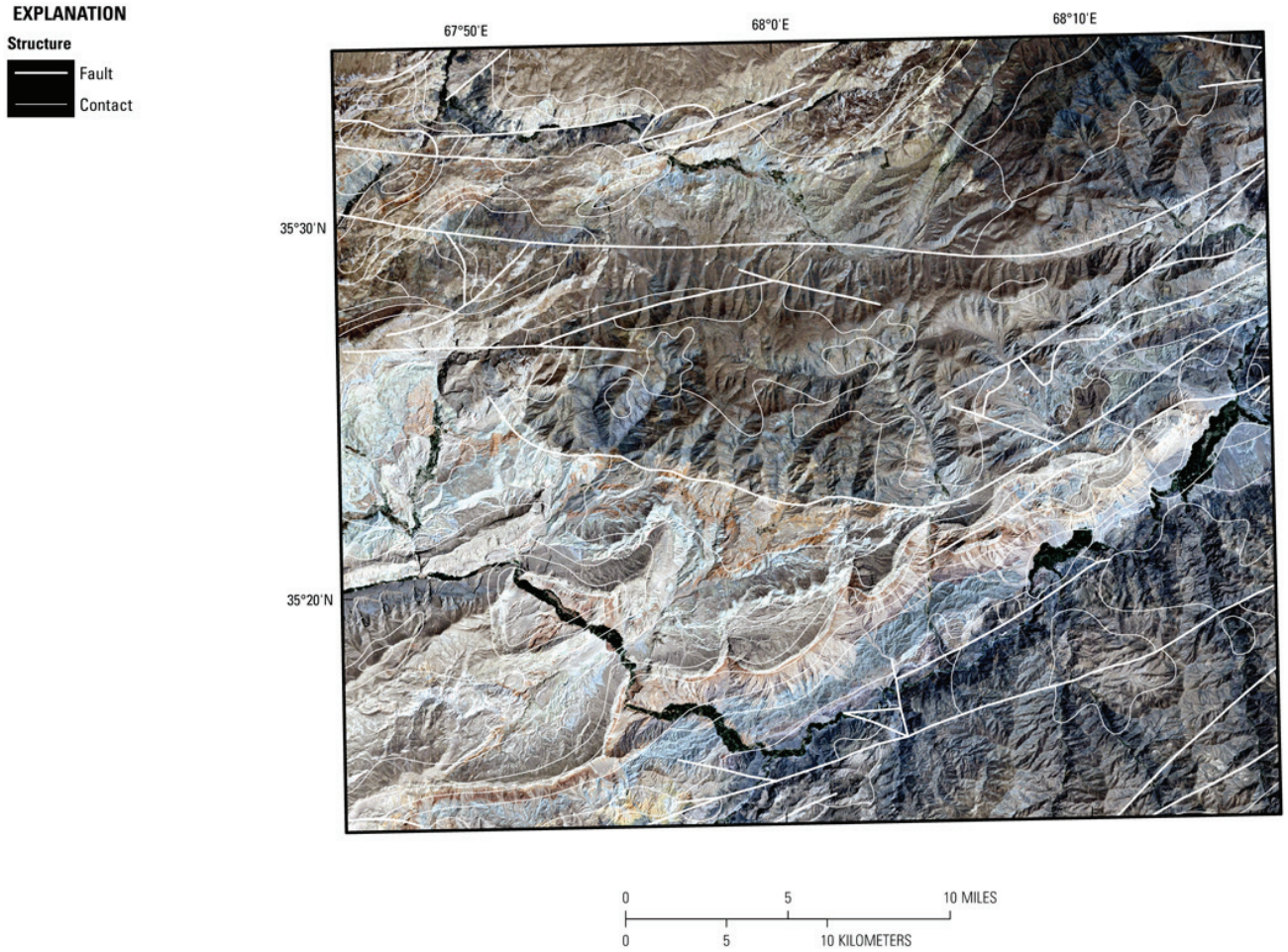

Figure 17B–2. Contrast-enhanced Landsat Thematic Mapper natural-color image of the Baghlan area of interest. Geology from digital geologic map of Afghanistan (Abdullah and Chmyriov, 1977; Doebrich and Wahl, 2006; Peters and others, 2007).

17B.3.1 Topography

Elevations in the Baghlan AOI range from 1,147 to 4,015 m (fig. 17B–3). The lowest areas within the Baghlan AOI are along the river that cuts through the southeastern region of the AOI. The highest elevations are found in the central and northern sections of the AOI. There are three population centers within the AOI: Ruyi Du Ab in the northeast, Tala Wa Barfak in the east, and Kahmard in the south.

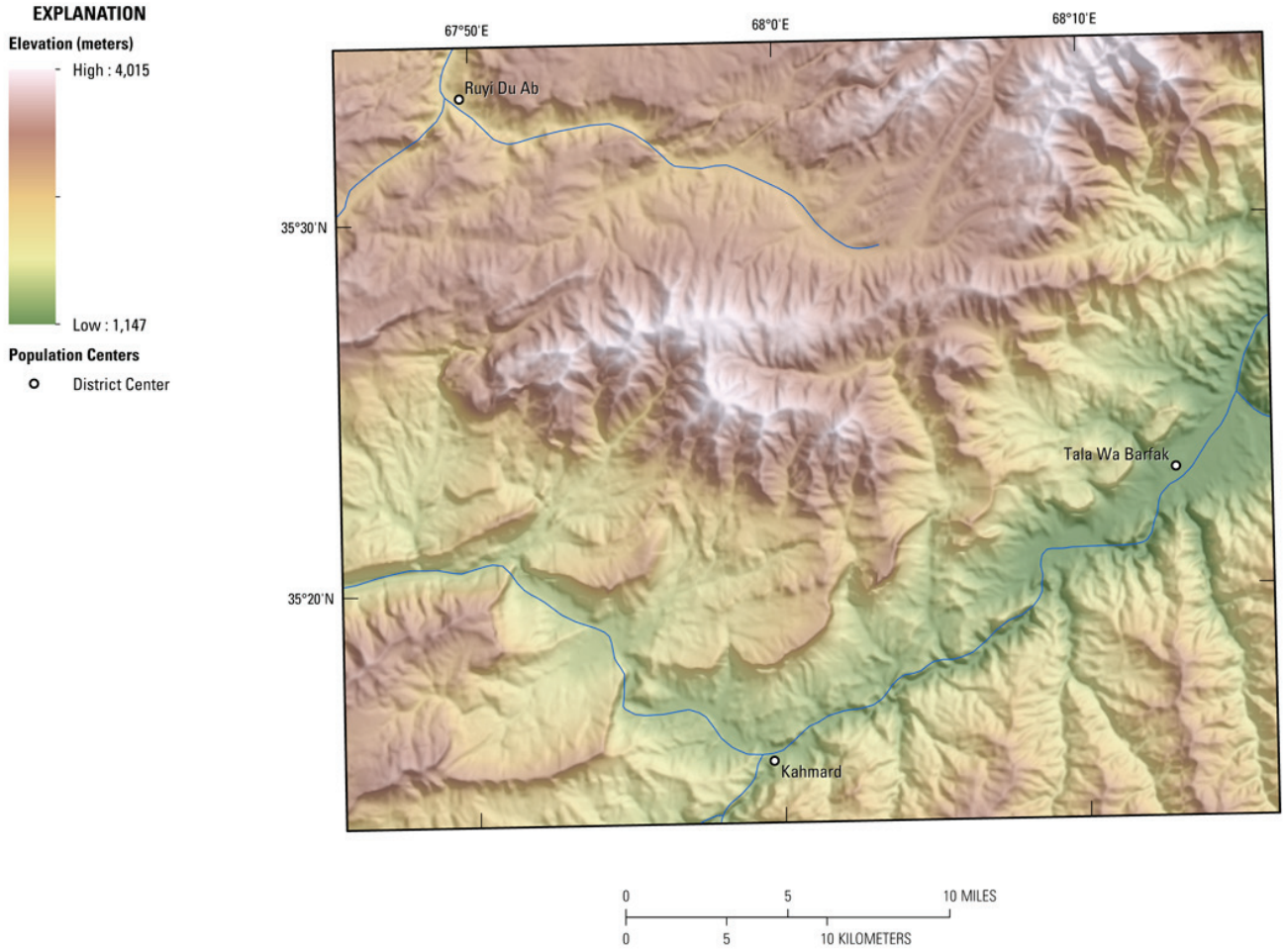

Figure 17B–3. Elevations and topography of the Baghlan area of interest.

17B.3.2 Lithology and Structure

Rocks in the Baghlan area range in age from Ordovician to Recent. The southeastern region of the AOI contains Paleozoic age rocks that are overlain by Triassic, Jurassic, and Cretaceous sedimentary rocks, which are in turn overlain in the central parts of the AOI by Eocene and Neogene age sedimentary rocks. Triassic granitic plutons and stocks intrude the older rocks in the eastern part of the AOI. Gypsum, clay, and bauxite deposits are most abundant in the Jurassic sedimentary rocks associated with coal (Peters and others, 2007). Gypsum also occurs in some Eocene age sedimentary rocks (fig. 17B–4; Abdullah and Chmyriov, 1977; Doebrich and Wahl, 2006; Peters and others, 2007).

17B.3.3 Known Mineralization

Figure 17B–5 shows 23 locations where mineralization with a potential for mineral resource development may exist (Peters and others, 2007). A number of different types of mineral prospects, particularly gypsum, clay, and bauxite prospects are present within the Baghlan AOI. The mineralogical

characteristics of the mineralized prospects are summarized in table 17B–1. There are also prospects of copper skarns, polymetallic veins, and sulfur, but these do not correlate well to the imaging spectroscopy data or are too small to be resolved.

The main known bauxite prospect is the Nalag prospect near lat 35°25'16"N., long 68°09'20"E. The prospect occurs in the weathering crust of Upper Triassic extrusive rocks at the base of a Jurassic coal-bearing sequence (Peters and others, 2007). Ten bauxite bodies, as thick as 4 m and as long as 200 m, have been identified in the area (Abdullah and others, 1977, Doebrich and Wahl, 2006; Peters and others, 2007). The main bauxite prospect is the Eshpushta prospect near lat 35°25'16"N., long 68°09'20"E. The prospect, ranging in thickness from 1 to 3 m and extending for 300–400 m, also occurs in the weathering crust of Upper Triassic extrusive rocks. The bauxites are light gray and pinkish (Abdullah and others, 1977, Doebrich and Wahl, 2006; Peters and others, 2007). A small occurrence of bauxite (Estoma Bauxite prospect) is present in the weathering crust of Upper Triassic extrusive rocks at the base of Jurassic coal-bearing sequence (Abdullah and others, 1977, Doebrich and Wahl, 2006; Peters and others, 2007).

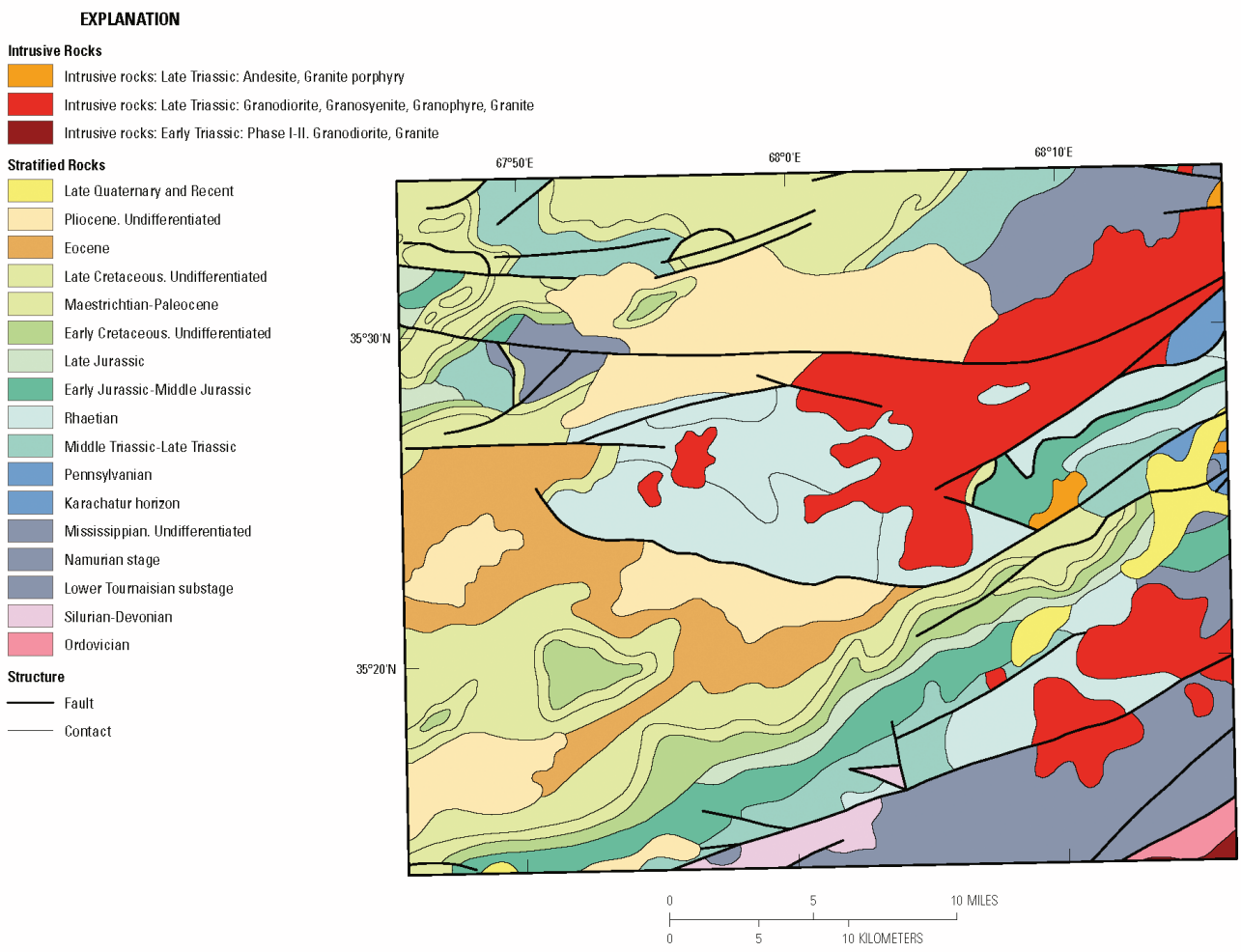

Figure 17B–4. Geologic map of the Baghlan area of interest from 1:500,000-scale geologic map of Afghanistan (Abdullah and Chmyriov, 1977; Doebrich and Wahl, 2006; Peters and others, 2007).

The main known gypsum occurrence is the Dasht-i-Safed Gypsum prospect located near lat 35°18'32"N., long 67°57'24"E. The prospect is a sulfur-bearing bed (1.0 to 1.5 m thick) containing celestite and lies between Upper Cretaceous–Paleocene marl and gypsum strata (Abdullah and others, 1977, Doebrich and Wahl, 2006; Peters and others, 2007). Gypsum prospects include the Nadr, Kamard,

Dasht-i-Safed, and Nalak prospects. The Nadr prospect near lat 35°26'25"N., long 67°48'02"E., is a 12-m-thick bed containing 89 percent gypsum that occurs in Upper Cretaceous–Paleocene dolomite, clay, and limestone that crop out from beneath Eocene prospects (Abdullah and others, 1977, Doebrich and Wahl, 2006; Peters and others, 2007). The Kahmard prospect is located near lat 35°18'32"N., long 67º54'E. This prospect contains beds consisting of massive gypsum, as much as 2.5 m thick, and stratified gypsum, 20 to 40 cm thick. The gypsum has been found in Upper Cretaceous–Paleocene clay and dolomite. The total thickness of the gypsum unit is 20 m and the average gypsum content is 97.94 weight percent (Abdullah and others, 1977, Doebrich and Wahl, 2006; Peters and others, 2007). The Dasht-i-Safed prospect is located near lat 35°17'09"N., long 67°53'08"E. This is a unit of stratified gypsum 30 m thick, occurring in Upper Cretaceous–Paleocene clay and limestone (Abdullah and others, 1977, Doebrich and Wahl, 2006; Peters and others, 2007). The Nalak prospect is a bedded gypsum prospect within Upper Jurassic sandstones and clays (Abdullah and others, 1977, Doebrich and Wahl, 2006; Peters and others, 2007).

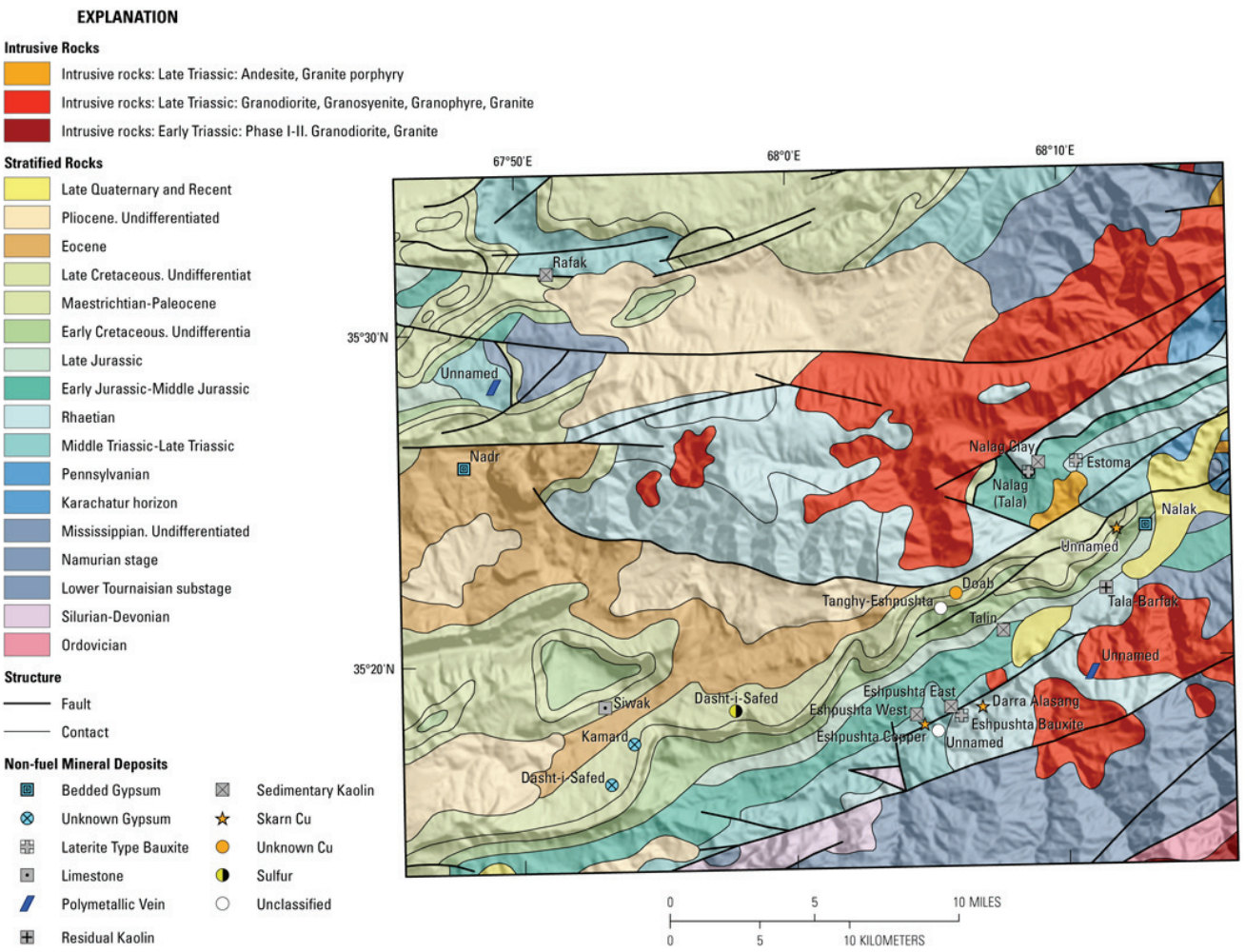

Figure 17B–5. Sites of known mineralization by deposit type (Abdullah and Chmyriov, 1977; Doebrich and Wahl, 2006; Peters and others, 2007) on the geologic map of the Baghlan area of interest from 1:500,000-scale geologic map of Afghanistan (Abdullah and Chmyriov, 1977; Doebrich and Wahl, 2006; Peters and others, 2007).

Table 17B–1. Known sites of mineralization in the Baghlan area of interest.

[Data are from Abdullah and Chmyriov (1977), Doebrich and Wahl (2006), and Peters and others (2007)]

Name	Deposit type	Major commodity	Host lithology	Alteration	Mineralogy	Gangue
Dasht-i-Safed Gypsum	unknown gypsum	Gyp	Upper Cretaceous - Paleocene clays and limestones	_	Gypsum	No data
Kamard Gypsum	unknown gypsum	Gyp	Upper Cretaceous - Paleocene clays and dolostone	_	Gypsum	No data
Unnamed	unclassified	Cu	Upper Triassic acidic effusives, tuff- sandstones and conglomerates	_	Chalcopyrite; malachite; sphalerite	No data
Eshpushta Copper	skarn Cu	Cu	Middle - Upper Triassic lime sandstones, gravelstones and conglomerates	Skarn alteration	Chalcopyrite; pyrite; arsenopyrite; sphalerite; molybdenite	No data
Eshpushta Bauxite	laterite-type bauxite	Al	Weathering profile over Upper Triassic effusives	Laterization	Bauxite	No data
Eshpushta West	sedimentary kaolin	China clay	Lower - Middle Jurassic terrigenous rocks	Kaolinization	No data	No data
Dasht-i-Safed Sulfur	sulfur	S	Sulfur bed between Upper Cretaceous - Paleocene marls and gypsum	_	Sulfur native; celestite	No data
Siwak	limestone	Limestone	Upper Cretaceous - Paleocene marls and marly limestones	_	No data	No data
Eshpushta East	sedimentary kaolin	China clay	Middle - Upper Triassic rocks	Kaolinization	No data	No data
Darra Alasang	skarn Cu	Cu Sn Pb	A contact of Upper Triassic granites and Upper Triassic shales	Skarn alteration	Pyrrhotite; chalcopyrite; sphalerite; galena; scheelite; cassiterite; ilmenite	No data
Unnamed	polymetallic vein	Cu	A contact of Upper Triassic granodiorites and Upper Triassic sandstones and volcanogenics	Silicification; pyritization	Pyrite	Quartz
Talin	sedimentary kaolin	Fireclay	Clays in Lower - Middle Jurassic deposits	_	No data	No data
Tanghy-Eshpushta	unclassified	Cu	Upper Cretaceous limestones and dolostone	Silicification; limonitization; malachitization	Limonite; jarosite; copper pitch ore; fahlore	Quartz
Doab	unknown Cu	Cu				
Tala-Barfak	residual kaolin	China clay	Kaolines in weathering profile over Upper Triassic quartz porphyry subvolcanic body	Kaolinization	Kaolin	No data
Unnamed	skarn Cu	Cu	A contact of Upper Cretaceous limestones	Skarn alteration of magnetite facies	Chalcopyrite; pyrite; magnetite	No data
Nalak Gypsum	bedded gypsum	Gyp	Upper Jurassic sandstones and clays	_	Gypsum	No data

Name	Deposit type	Major commodity	Host lithology	Alteration	Mineralogy	Gangue
Nalag (Tala)	laterite-type bauxite	Al	Weathering profile over Upper Triassic effusives in the bottom of overlaying Jurassic coal-bearing deposits	Laterization	Bauxite	No data
Nadr	bedded gypsum	Gyp	Upper Cretaceous - Paleocene dolostone, clays and limestones exposed among Eocene deposits	_	Gypsum	No data
Nalag Clay	sedimentary kaolin	Fireclay	Clays on Upper Triassic diorites porphyry	_	Not data	No data
Estoma Bauxite	laterite type bauxite	Al	Weathering profile over Upper Triassic effusives in the bottom of overlying Jurassic coal-bearing deposits	Laterization	Bauxite	No data
Unnamed	polymetallic vein	Cu	Middle - Upper Triassic deposits	Silicification	Pyrite; hematite; limonite; quartz	Quartz
Rafak	sedimentary kaolin	Fireclay	clays among Lower Cretaceous siltstones	_	No data	No data

The main known kaolinite occurrence is the Tala-Barfak prospect near lat 35°21'49"N., long 68°10'40"E. The prospect consists of three small kaolin relics in the weathering crust on a Late Triassic subvolcanic body of quartz porphyry (Peters and others, 2007; Abdullah and others, 1977). The kaolin relics extend for more than 1 km, their widths reaching 250 m, and thicknesses as much as 20 m. The kaolin is white, relatively compact, and at places includes patches of slightly weathered rock. Other kaolinite and clay prospects include the Eshpushta East prospect, which is a zone of slightly kaolinized rocks of Middle–Late Triassic age, 20 to 25 m thick that extends for 0.5 km (Abdullah and others, 1977, Doebrich and Wahl, 2006; Peters and others, 2007). The Eshpushta West prospect is a zone of slightly kaolinized rocks of Early–Middle Jurassic age that is 20 m thick and extends for 300 m (Abdullah and others, 1977, Doebrich and Wahl, 2006; Peters and others, 2007). The Rafak prospect is a 5-m-thick clay bed that occurs in Lower Cretaceous siltstone (Abdullah and others, 1977, Doebrich and Wahl, 2006; Peters and others, 2007). Other small prospects include the Nalag Clay and Talin prospects.

17B.4 Mineral Maps of the Baghlan Area of Interest

Analysis of the HyMap imaging spectrometer data of the Baghlan AOI using spectroscopic methods resulted in the identification of a wide variety of surficial minerals. Although the occurrence of certain minerals may suggest that mineralization processes may have once operated in the area, many of the minerals that were identified are also common rock-forming minerals or minerals that can be derived from the weathering of a wide variety of rock types. Consequently, the distribution patterns of the identified minerals and the geologic context in which they occur are extremely important in understanding the causes of mapped mineral occurrences and evaluating the possible potential for related mineral prospects. The presence of abundant vegetation, which masked the surficial minerals in significant parts of the area, has reduced the utility of the imaging spectroscopy data for overall site characterization in several regions within the Baghlan AOI.

Figure 17B–6 depicts the results of the MICA analyses of the HyMap data for the Baghlan AOI for the 2-µm materials, which include clays, carbonates, phyllosilicates, sulfates, altered minerals, and other materials. Carbonates cover most of the Baghlan AOI, primarily indicated by pixels containing calcite and calcite mixed with clay/mica. Pixels matching pure muscovite or illite standards occur over large contiguous areas in the central and southwestern areas. In the southwestern section, the muscovites and illites occur along a river basin. Distinct patterns of kaolinitic clays occur in bedded units primarily in the Early–Middle Jurassic stratified rock units. Bedded units, 30 km long and as much as 3 km wide, occur in the south-central and southeastern areas of the AOI along the river basin in Early–Middle Jurassic stratified units. Localized areas of kaolinite occur in the east-central, west-central and northwestern portions of the AOI mainly in Early–Middle Jurassic stratified rocks with smaller occurrences in Eocene and Rhaetian (Upper Triassic) stratified units. Large areas of epidote or chlorite were found throughout the AOI in Triassic and Carboniferous stratified units (see fig. 17B–6). Montmorillonite does map throughout the AOI in localized patterns, mainly in Eocene rocks, in the west-central portion of the AOI. Dolomite, serpentine or calcite + dolomite, and serpentine concentrations were mapped together throughout the AOI in what appears to be bedded units in many different lithologies.

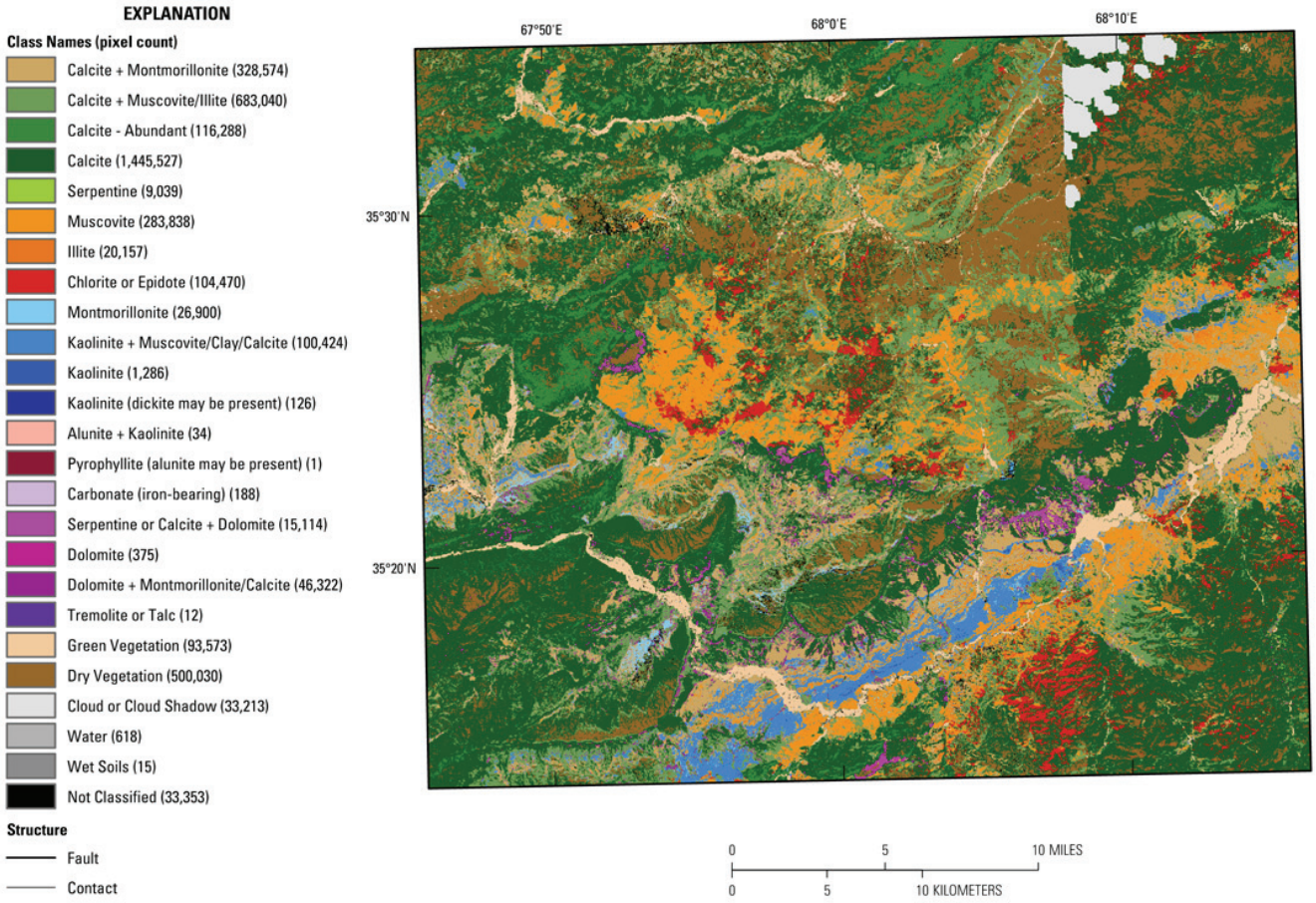

Figure 17B–6. Map of carbonates, phyllosilicates, sulfates, altered minerals, and other materials derived from HyMap data in the Baghlan area of interest.

Figure 17B–7 shows the results for the iron-bearing materials. The iron-bearing materials map is dominated by Fe^{2+} Fe^{3+}, Type 2, goethites, Fe^{2+}, Type 1, and hematite with smaller occurrences of epidote and Fe^{3+}, Type 1. Fe^{2+} Fe^{3+}, Type 2 dominate the Early–Middle Jurassic and Middle–Late Triassic rock units but also occur within the Eocene and Rhaetian strata. Fe^{2+} Fe^{3+}, Type 2 are coincident with the location of the 2 µm materials muscovites and illites. Goethites occur in Early–Middle Jurassic and Middle–Late Triassic bedded units in the southeast region of the AOI. Hematites and Fe^{3+} minerals map within the Early Cretaceous and Pliocene age rocks. Jarosite pixels map in small spatially cohesive clusters in the Middle Triassic-Late Triassic stratified units in the south-central region of the AOI.

Because of the large number of classes and the subtleties of the distribution patterns represented in these image maps, it is instructive to display these results as a series of image maps, each depicting a selected group of minerals that are mineralogically related or commonly occur together in special geologic environments (figs. 17B–8 to 17B–12). Figure 17B–8 shows the distribution of carbonate minerals in the Baghlan AOI, whereas figure 17B–9 shows where clay minerals and micas occur. The distribution of iron-oxide and iron-hydroxide minerals are displayed in figure 17B–10. Minerals commonly found in hydrothermally altered rocks are mapped in figure 17B–11, and secondary minerals often associated with mineralized and (or) weathered rocks are mapped in figure 17B–12.

17B.4.1 Carbonate Minerals

Carbonate minerals, either calcite or dolomite, were mapped over a large portion of the Baghlan AOI (fig. 17B–8). In general, the carbonates are mapped throughout the AOI and within almost every geologic unit. Dolomite, serpentine or calcite + dolomite, and serpentine occurrences were mapped

together throughout the southern region of the AOI in what appears to be bedded units in many different strata. The known limestone prospect of Siwak occurs within a calcite unit in the southwest region of the AOI.

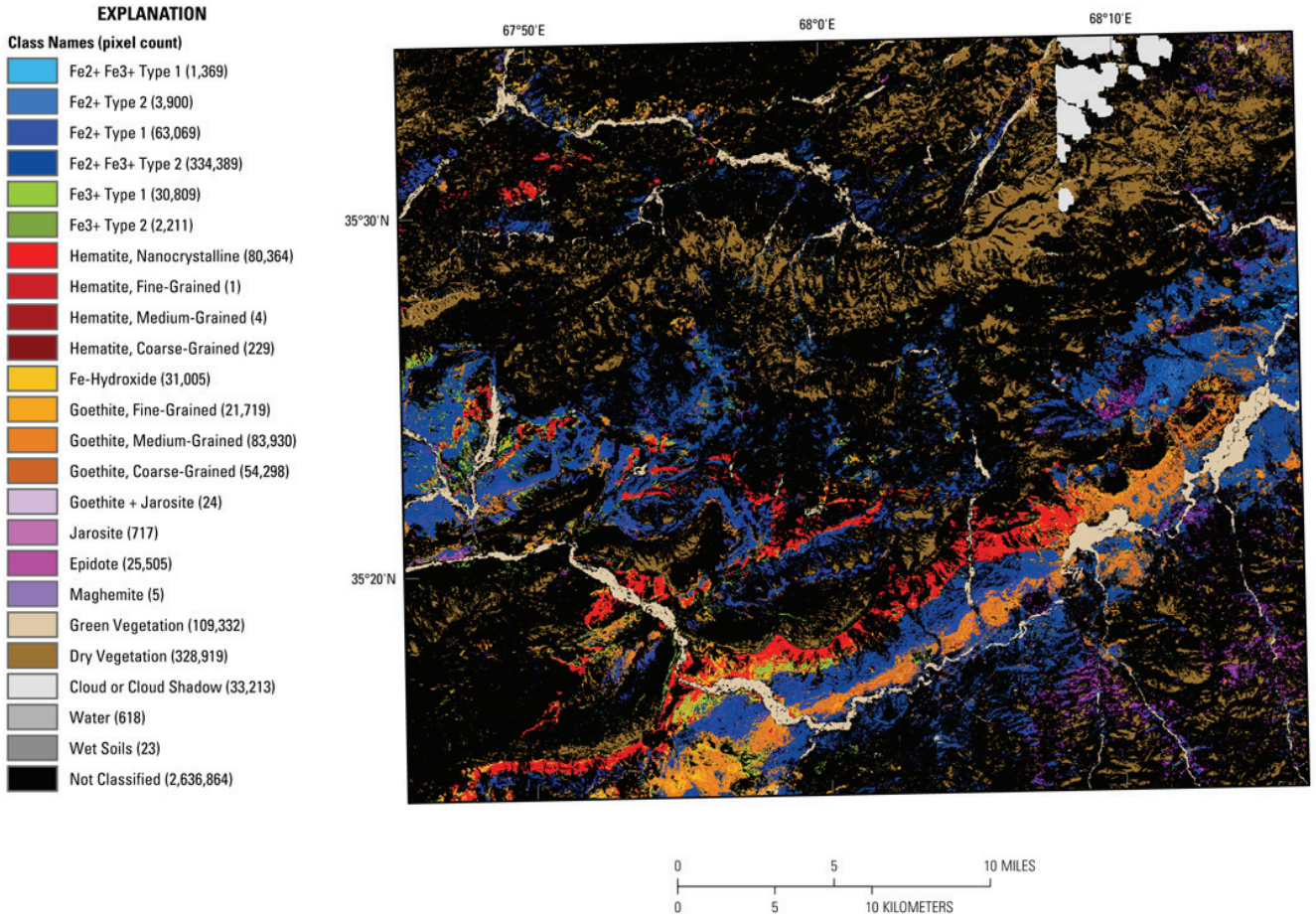

Figure 17B–7. Map of iron-bearing minerals and other materials derived from HyMap data in the Baghlan area of interest.

17B.4.2 Clays and Micas

Pixels matching pure muscovite or illite spectra occur over large contiguous areas in the central and southwest areas of the AOI. In the southwestern section, muscovites and illites occur along a river basin. Distinct patterns of kaolinite clays occur in localized patterns and in bedded units mainly in the Early Jurassic-Middle Jurassic stratified units. Extensive bedded units of kaolinite and muscovite 30 km long and as much as 3 km wide occur in the south-central and southeastern areas of the AOI along the river basin in Early–Middle Jurassic and Middle–Late Triassic age rocks. Localized areas of spatially related kaolinite occur in the east-central, west-central, and northwestern portions of the AOI mainly in Early–Middle Jurassic and Middle–Late Triassic age rocks with smaller occurrences in Eocene and Rhaetian stratified units. The Tala-Barfak, Eshpushta West, and Eshpushta East kaolinite prospects did map within units of kaolinite detected by HyMap data. Interestingly, Tala-Barfak, Eshpushta West, and Eshpushta East are considered China clay commodities and were mapped as kaolinite where the Talin, Nalag Clay and Rafak kaolinite prospects are described as fire-clay commodities and mapped mainly within calcite or calcite/dolomite units (Abdullah and Chmyriov, 1977; Doebrich and Wahl, 2006; Peters and others, 2007). Large areas of epidote or chlorite were found throughout the AOI in Triassic and Carboniferous age stratified units (see fig. 17B–6). Montmorillonite does map throughout the AOI

in localized patterns mainly in the Eocene unit in the west-central portion of the AOI. Alunite + kaolinite maps as individual pixels, but those pixels are limited to the southeast region of the AOI.

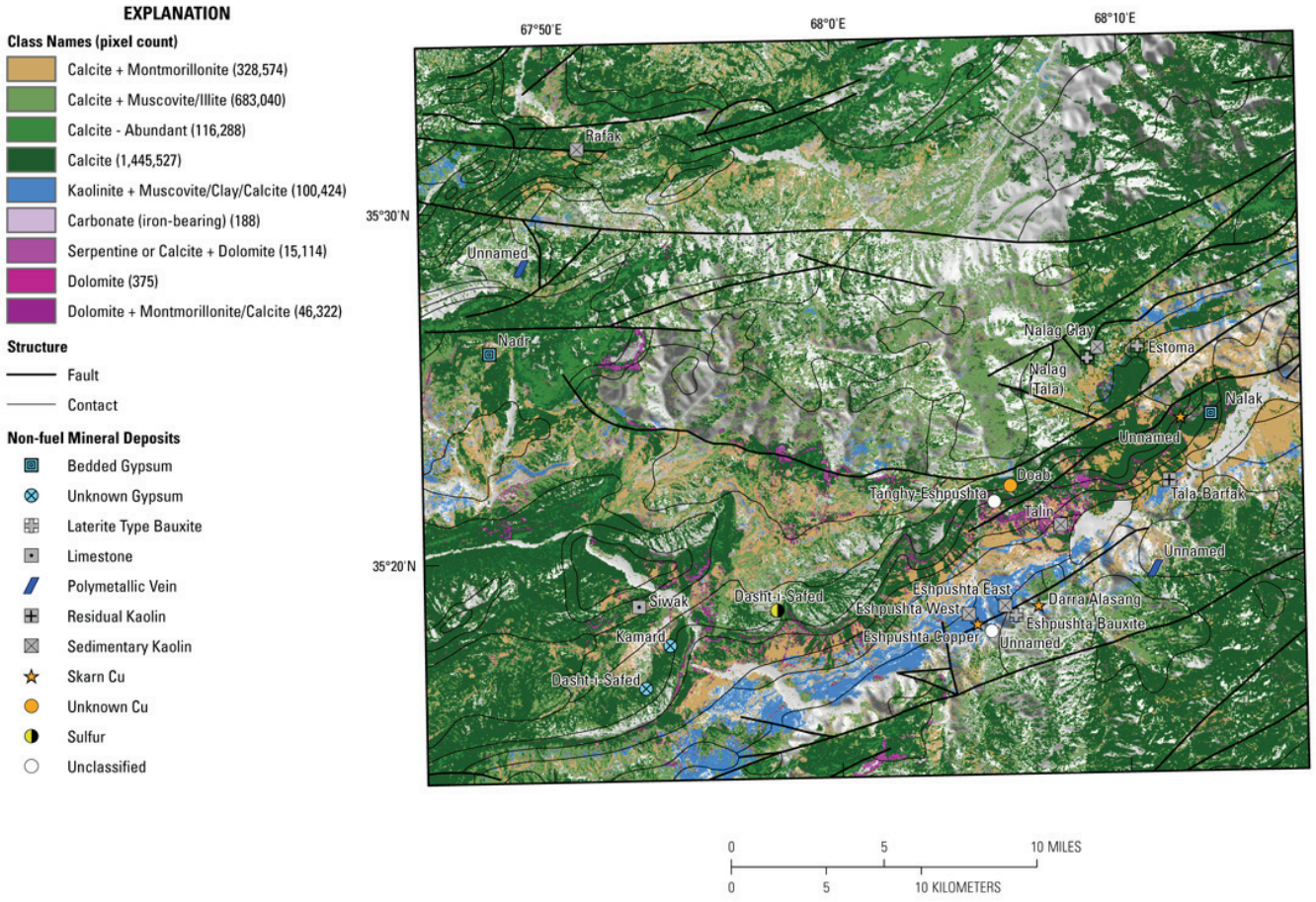

Figure 17B–8. Map of distribution of carbonate minerals derived from HyMap data in the Baghlan area of interest.

17B.4.3 Iron Oxides and Iron Hydroxides

The Baghlan AOI contains large areas of hematite in the southern region of the area (fig. 17B–10) in Early Cretaceous strata. The description of the Early Cretaceous units includes redstone and is consistent with the HyMap hematite classes (Abdullah and Chmyriov, 1977; Doebrich and Wahl, 2006; Peters and others, 2007). Goethite and Fe-hydroxide are observed across the AOI in bedded lithologies running parallel to the hematite with the largest concentration in the southern part of the AOI. Goethite in the Baghlan AOI approximately coincide with areas where kaolinites are mapped in the 2-µm materials map. Jarosite is found in small concentrations but is consistently found within the Middle–Late Triassic age unit. Jarosite is bordered by the goethite classes in the iron-bearing map and is mainly associated with kaolinites in the clays, carbonates, phyllosilicates, sulfates, altered minerals, and other materials map (near lat 35°18'26"N., long 68°04'48"E.). Occurrences of epidote are found dispersed over the AOI in several different geologic units.

17B.4.4 Common Alteration Minerals

Most of the minerals in this group are commonly present in hydrothermally altered rocks associated with epithermal mineral deposits (fig. 17B–11). Consequently, where they occur in distinct clusters is of great interest in terms of potential mineral deposits. However, the minerals do not occur in distribution patterns that are suggestive of such alteration in the Baghlan AOI. All of the mineral classes

in this map with the exception of kaolinite (dickite may be present) occur over large areas with little spatial coherence in the AOI. Kaolinite (dickite may be present) did cluster in two locations; one near lat 35°20'12"N., long 68°05'49"E., and the second near lat 35°19'27"N., long 68°07'50"E., which should be examined in more detail in future studies.

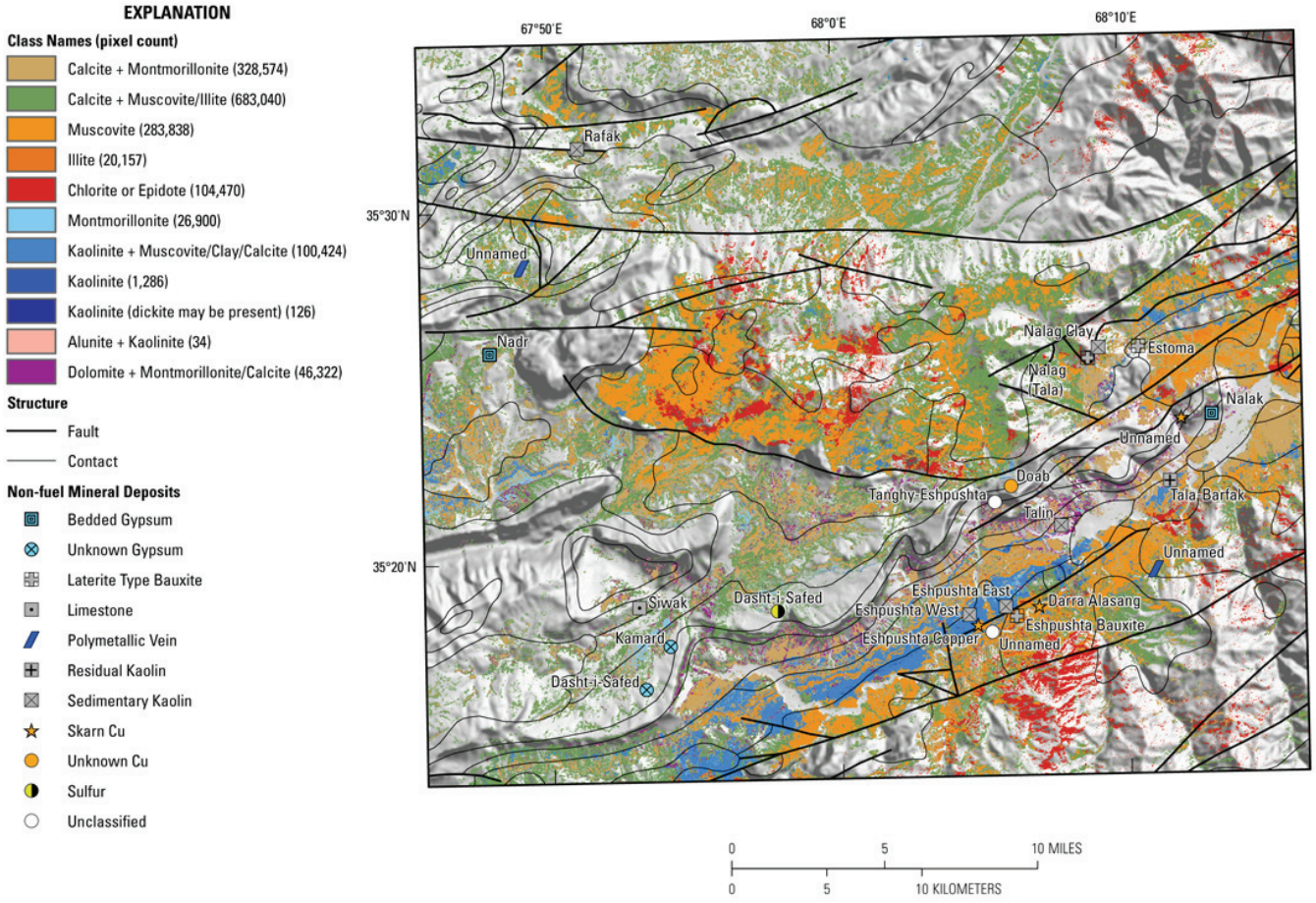

Figure 17B–9. Map of distribution of clay and mica minerals derived from HyMap data in the Baghlan area of interest.

17B.4.5 Common Secondary Minerals

Secondary minerals, in the epidote and chlorite or epidote classes (fig. 17B–12), are distributed throughout the AOI. Serpentine and serpentine or calcite + dolomite occur in association with dolomites in the southeast and west-central regions of the AOI.

17B.4.6 Gypsum

A specialized MICA analysis to enhance the detection and map the spatial distribution of gypsum was completed for the AOI. The result of that mapping is shown in figure 17B–13, in which gypsum is most prominent in the center of the Baghlan AOI. Small groupings and single pixel detections occur south-southwest and north-northeast of the central concentration in similar geologic units. Gypsum was detected near the known gypsum prospects of Kamard, Dasht-i-Safed, Nadr, and Nalak. With the exception of Nalak, only a few pixels of gypsum are detected near the known mineral occurrences. At Nalak, the analysis of imaging spectrometer data revealed an area containing gypsum more than 110 hectares in size. Additional concentrations of pixels with strong gypsum-related absorption features in their spectra occur near lat 35°22'28"N., long 68°05'57"E., within an area greater than 100 hectares and near lat 35°19'50"N., long 68°01'03"E., in a narrow zone 3 km in length. These

previously unreported gypsum concentrations in the center of the AOI are discussed in more detail in King, Johnson, and others (2011).

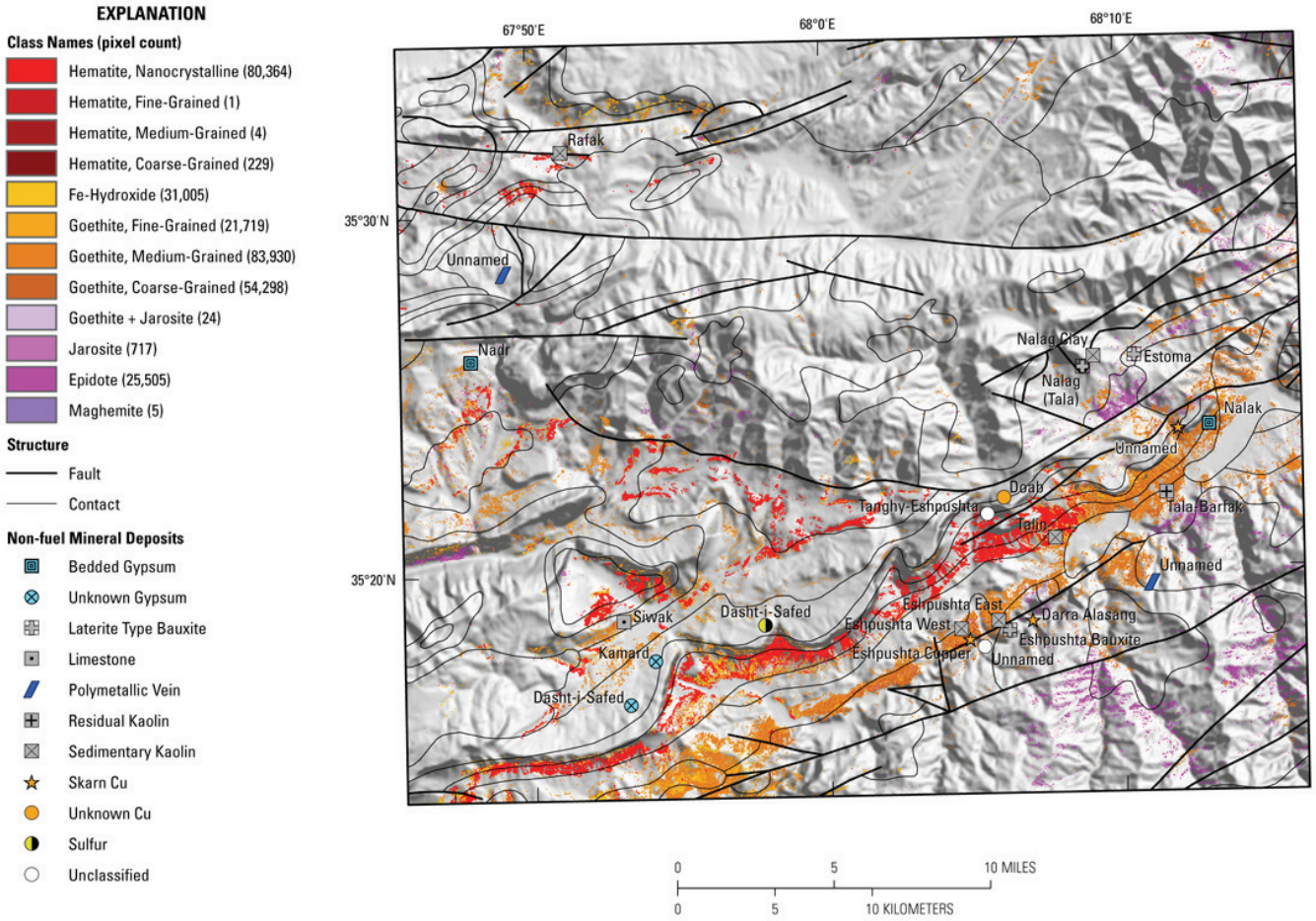

Figure 17B–10. Map of distribution of iron oxide and iron hydroxide derived from HyMap data in the Baghlan area of interest.

17B.5 Summary

Carbonate minerals and vegetation cover most of the Baghlan AOI. Muscovites and illites were detected in greatest concentration in the mapped units of Triassic and Jurassic rocks in the central to southeastern region of the Baghlan AOI and in smaller patches to the northwest. Epidote and chlorite were found in spatially consistent patterns in the central and southeast regions. Kaolinites were distributed within the Early–Middle Jurassic and Middle–Late Triassic age stratified units. A large occurrence of kaolinite was mapped in the southern part of the AOI. In the iron-bearing materials map, the goethites approximately coincide with areas where kaolinites are mapped in the 2-µm map, and the Fe^{2+} Fe^{3+}, Type 2 are coincident with the location of the 2-µm muscovites and illites. The hematites consistently map within geologic units described as red sandstone. Jarosite is found in small concentrations throughout the goethite classes in the Middle–Late Triassic age geologic unit. In most locations jarosite correlates to kaolinite in the 2-µm map. A customized MICA analysis for gypsum was performed to better define their spatial distribution. The analysis yielded detections consistent with known gypsum occurrences at Kamard, Dasht-i-Safed, Nadr, and Nalak and identified several previously unknown concentrations of pixels that warrant additional investigation. The bauxite mineral occurrences did not seem to correlate to specific minerals detected by HyMap, but the addition of bauxite minerals to the spectral library could improve our detections. Kaolinite detections were

consistent with the China clay-type kaolinites in the Tala-Barfak, Eshpushta West, and Eshpushta East prospects.

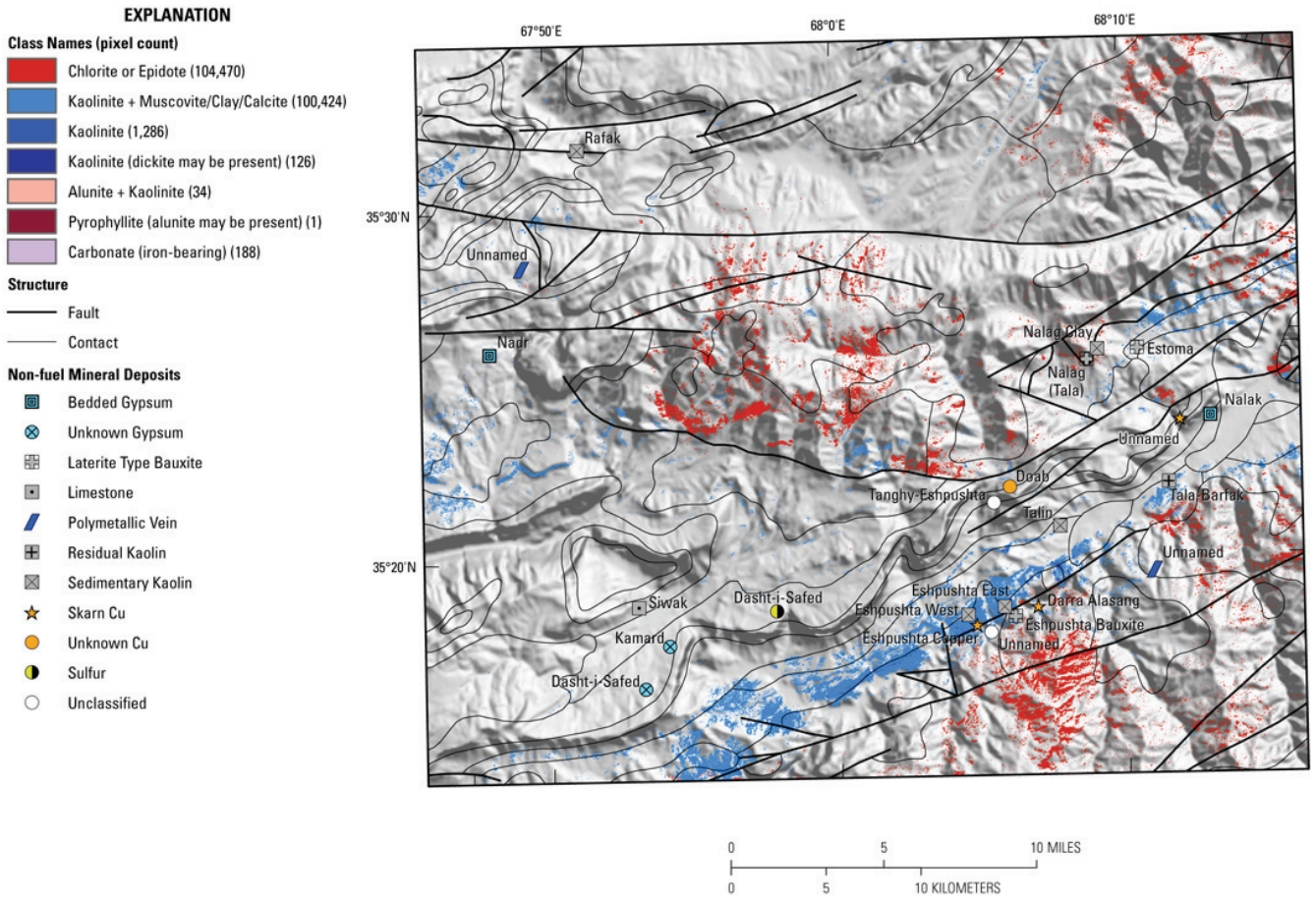

Figure 17B–11. Map of distribution of common alteration minerals derived from HyMap data in the Baghlan area of interest.

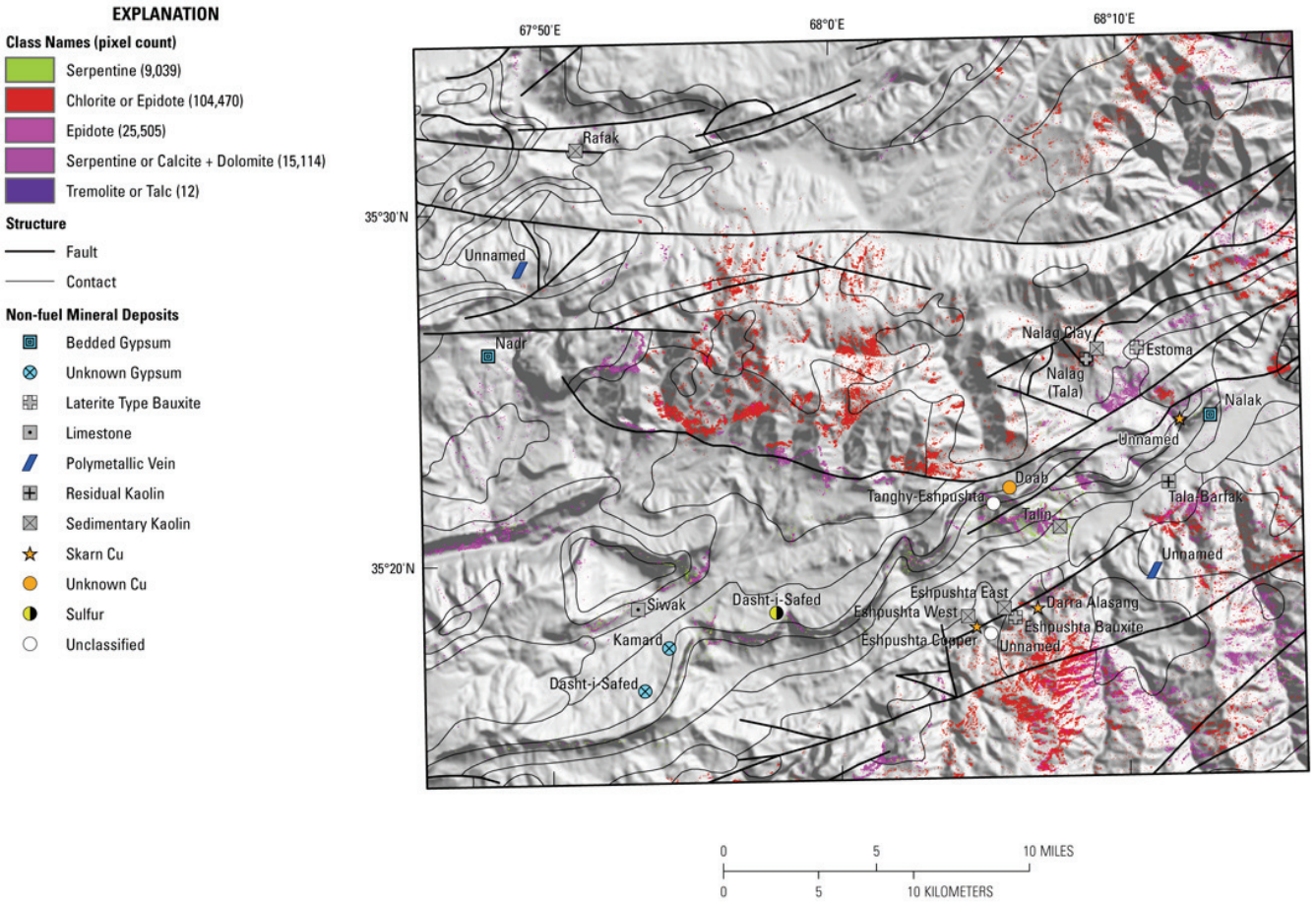

Figure 17B–12. Map of distribution of common secondary minerals derived from HyMap data in the Baghlan area of interest.

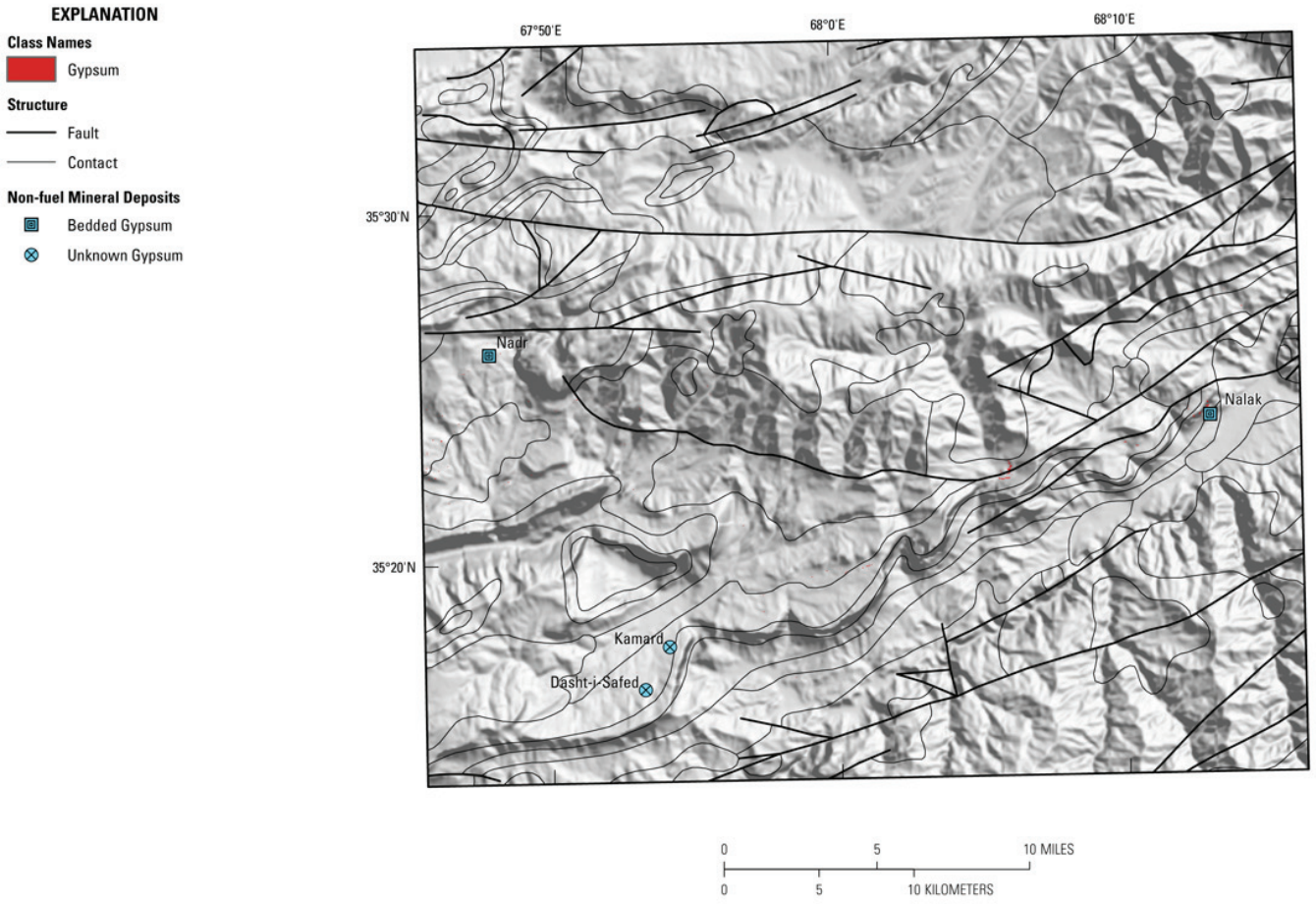

Figure 17B–13. Map of gypsum distribution derived from HyMap data in the Baghlan area of interest.

17B.6 References Cited

Abdullah, Sh., and Chmyriov, V.M., eds., 1977, Map of mineral resources of Afghanistan: Kabul, Afghanistan, Ministry of Mines and Industries of the Democratic Republic of Afghanistan, Department of Geological and Mineral Survey, V/O "Technoexport" USSR, scale 1:500,000.

Abdullah, Sh., Chmyriov, V.M., Stazhilo-Alekseev, K.F., Dronov, V.I., Gannan, P.J., Rossovskiy, L.N., Kafarskiy, A.Kh., and Malyarov, E.P., 1977, Mineral resources of Afghanistan (2d ed.): Kabul, Afghanistan, Republic of Afghanistan Geological and Mineral Survey, 419 p.

Cocks, T., Jenssen, R., Stewart, A., Wilson, I., and Shields, T., 1998, The HyMap airborne hyperspectral sensor—The system, calibration and performance, *in* Schaepman, M., Schlapfer, D., and Itten, K.I., eds., Proceedings of the 1st EARSeL Workshop on Imaging Spectroscopy, 6–8 October 1998, Zurich: Paris, European Association of Remote Sensing Laboratories, p. 37–43.

Davis, P.A., 2007, Landsat ETM+ false-color image mosaics of Afghanistan: U.S. Geological Survey Open-File Report 2007–1029, 22 p. (Also available at *http://pubs.usgs.gov/of/2007/1029/*.)

Doebrich, J.L., and Wahl, R.R., comps., *with contributions by* Doebrich, J.L., Wahl, R.R., Ludington, S.D., Chirico, P.G., Wandrey, C.J., Bohannon, R.G., Orris, G.J., Bliss, J.D., and ____, 2006, Geologic and mineral resource map of Afghanistan: U.S. Geological Survey Open File Report 2006–1038, scale 1:850,000, available at *http://pubs.usgs.gov/of/2006/1038/*.

Hoefen, T.M., Kokaly, R.F., and King, T.V.V., 2010, Calibration of HyMap data covering the country of Afghanistan, *in* Proceedings of the 15th Australasian Remote Sensing and Photogrammetry Conference, Alice Springs, Australia, September 12–17, 2010, p. 409, available at *http://dl.dropbox.com/u/81114/15ARSPC-Proceedings.zip/*.

King, T.V.V., Johnson, M.R., Hoefen, T.M., Kokaly, R.F., and Livo, K.E., 2011, Mapping potential mineral resource anomalies using HyMap data, *in* King, T.V.V., Johnson, M.R., Hubbard, B.E., and Drenth, B.J., eds, Identification of mineral resources in Afghanistan—Detecting and mapping resource anomalies in prioritized areas using geophysical and remote sensing (ASTER and HyMap) data in Afghanistan: U.S. Geological Survey Open-File Report 2011–1229, available at *http://pubs.usgs.gov/of/2011/1229/*.

King, T.V.V., Kokaly, R.F., Hoefen, T.M., Dudek, K. and Livo, K.E., 2011, Surface materials map of Afghanistan—Iron-bearing minerals and other materials: U.S. Geological Survey Scientific Investigations Map 3152–B.

King, T.V.V., Kokaly, R.F., Hoefen, T.M., and Knepper, D.H., 2010, Resource mapping in Afghanistan using HyMap data, *in* Proceedings of the 15th Australasian Remote Sensing and Photogrammetry Conference, September 12–17, 2010, Alice Springs, Australia, p. 500, available online at http://dl.dropbox.com/u/81114/15ARSPC-Proceedings.zip/.

Kokaly, R.F., King, T.V.V., and Livo, K.E., 2008, Airborne hyperspectral survey of Afghanistan 2007—Flight line planning and HyMap data collection: U.S. Geological Survey Open-File Report 2008–1235, 14 p.

Kokaly, Ray, 2011, PRISM—Processing routines in IDL for spectroscopic measurements: U.S. Geological Survey Open-File Report 2011–1155, available at *http://pubs.usgs.gov/of/2011/1155/*.

Kokaly, R.F., King, T.V.V., Hoefen, T.M., Dudek, K. and Livo, K.E., 2011, Surface materials map of Afghanistan—Carbonates, phyllosilicates, sulfates, altered minerals, and other materials: U.S. Geological Survey Scientific Investigations Map 3152–A.

Peters, S.G., Ludington, S.D., Orris, G.J., Sutphin, D.M., Bliss, J.D., and Rytuba, J.J., eds., and the U.S. Geological Survey-Afghanistan Ministry of Mines Joint Mineral Resource Assessment Team, 2007, Preliminary non-fuel mineral resource assessment of Afghanistan: U.S. Geological Survey Open-File Report 2007–1214, 810 p., 1 CD–ROM. (Also available at *http://pubs.usgs.gov/of/2007/1214/*.)